

Lattice dynamics in magnetic superelastic Ni-Mn-In alloys. Neutron scattering and ultrasonic experiments

Xavier Moya[†], David González-Alonso, Lluís Mañosa* and Antoni Planes
*Departament d'Estructura i Constituents de la Matèria, Facultat de Física,
 Universitat de Barcelona, Diagonal 647, E-08028 Barcelona, Catalonia, Spain*

V. O. Garlea, T. A. Lograsso, D. L. Schlager and J. L. Zarestky
Ames Laboratory, Iowa State University, Ames, Iowa 50011

Seda Aksoy and Mehmet Acet
Fachbereich Physik, Experimentalphysik, Universität Duisburg-Essen, D-47048 Duisburg, Germany
 (Dated: June 19, 2009)

Neutron scattering and ultrasonic methods have been used to study the lattice dynamics of two single crystals of Ni-Mn-In Heusler alloys close to $\text{Ni}_{50}\text{Mn}_{34}\text{In}_{16}$ magnetic superelastic composition. The paper reports the experimental determination of the low-lying phonon dispersion curves and the elastic constants for this alloy system. We found that the frequencies of the TA_2 branch are relatively low and it exhibits a small dip anomaly at a wave number $\xi_0 \approx 1/3$, which softens with decreasing temperature. Associated with the softening of this phonon, we also observed the softening of the shear elastic constant $C' = (C_{11} - C_{12})/2$. Both temperature softenings are typical for bcc based solids which undergo martensitic transformations and reflect the dynamical instability of the cubic lattice against shearing of $\{110\}$ planes along $\langle 1\bar{1}0 \rangle$ directions. Additionally, we measured low-lying phonon dispersion branches and elastic constants in applied magnetic fields aimed to characterize the magnetoelastic coupling.

PACS numbers: 81.30.Kf, 63.20.-e, 64.70.Kb, 62.20.Dc

I. INTRODUCTION

The search of magnetic shape memory alloys with more favourable mechanical properties than Ni_2MnGa has prompted in recent years the study of new Ni-Mn based Heusler alloys, extending this alloy family to other elements of groups IIIA-VA [1, 2, 3, 4]. Among them, Ni-Mn-In system has drawn much attention due to the large shift of the martensitic transition temperatures by an applied magnetic field observed in $\text{Ni}_{50}\text{Mn}_{34}\text{In}_{16}$ (~ 10 K/T), as a consequence of a strong spin-lattice coupling at a microscopic level [5]. These large shifts allow for the application of moderate magnetic fields to induce the structural transition and lead to many functional properties such as the magnetic superelasticity [5], large inverse magnetocaloric effects [6, 7, 8] and magnetoresistance [9].

From a fundamental point of view, many of the Ni-Mn based alloys exhibit singular lattice-dynamical behavior associated with the martensitic transition from a high temperature cubic phase to a lower symmetry martensitic phase. Specifically, in the case of Ni-Mn-Ga and Ni-Mn-Al alloys, it has been experimentally shown that the transverse TA_2 branch shows a dip at a particular wave number (anomalous phonon). The energy of such anomalous phonon softens with decreasing the temperature [10, 11, 12, 13, 14, 15]. The temperature dependence of the energy of the anomalous phonon parallels

that of the elastic constant $C' = (C_{11} - C_{12})/2$ which also softens with decreasing temperature [16, 17, 18, 19]. Softening observed both with neutron scattering and ultrasonic methods are typical for bcc based solids which undergo martensitic transformations and reflect the dynamical instability of the cubic lattice against shearing of $\{110\}$ planes along the $\langle 1\bar{1}0 \rangle$ directions [20]. In addition, significant magnetoelastic coupling exists in these systems as evidenced by the enhancement of the anomalous phonon softening when the sample orders ferromagnetically [12, 13], and by the change in the elastic constants when a magnetic field is applied [19, 21].

The study of the lattice dynamics of a broader class of Ni-Mn based compounds is important for a deeper understanding of the physical mechanisms behind the multifunctional properties of martensitic Heusler alloys. Therefore, much effort has been devoted in recent years to extend the study of the lattice dynamics to alloys other than Ni-Mn-Ga and Ni-Mn-Al by means of first principles calculations [22, 23]. In particular, Entel *et al.* have shown that the application of a magnetic field leads to the gradual vanishing of the phonon instability in the low-lying TA_2 branch for stoichiometric Ni_2MnIn , thus stabilizing the high temperature cubic phase [23]. The aim of the present work is to extend the experimental study of the lattice dynamics of this alloy-family to the Ni-Mn-In system, both in the short-wavelength and the long-wavelength limit by measuring the phonon dispersion branches and the elastic constants. Due to the strong interplay between magnetic and structural degrees of freedom typically exhibited by these compounds, we

*Electronic address: lluis@ecm.ub.es

carried out both kinds of experiments in applied magnetic field.

The paper is organized as follows: In Section II we describe the details of single crystal preparation and experimental techniques. Section III is devoted to the experimental results and is split into three sections, which describe the calorimetric (III A), phonon dispersion (III B) and elastic constants (III C) results. Finally, in Section IV we summarize and conclude.

II. EXPERIMENTAL DETAILS

A. Sample preparation

The single crystals were synthesized at the Materials Preparation Center, Ames Laboratory, USDOE [24]. Two single crystals with similar compositions were prepared, one for neutron scattering experiments and another one for ultrasonic experiments. Appropriate quantities of high purity nickel, manganese and indium were used to make these alloys. The electrolytic manganese was pre-arc melted to outgas it before alloying it with the other metals. The metals were arc melted several times under an argon atmosphere, flipping the buttons each time. The buttons were then remelted and the alloy drop cast into a copper chill cast mold to ensure compositional homogeneity throughout the ingots. The crystals were grown in a resistance furnace from the as-cast ingots in an alumina Bridgman style crucible. The ingots were heated under a pressure of 5.0×10^{-6} torr up to 1000 °C and 900 °C, for the neutron scattering and ultrasonic method samples, respectively, to degas the crucible and charge. The chamber was then backfilled to a pressure of 2.8×10^3 kPa with high purity argon. This over-pressurization was done near melting to diminish gas pockets from being trapped in the cone region of the crystal and also to minimize the amount of manganese evaporation from the melt during crystal growth. The ingots were further heated to 1250 °C and 1200 °C, for the neutron scattering and ultrasonic measurements samples, respectively, and held at this temperature for 1 hour to allow thorough mixing before withdrawing the samples from the heat zone at a rate of 5 mm/hr. The as-grown ingots were heat treated at 900 °C for 1 week and cooled at a rate of 10 °C/min. The average composition of the alloys were determined by energy dispersive X-ray analysis (EDX) to be $\text{Ni}_{49.3}\text{Mn}_{34.2}\text{In}_{16.5}$ and $\text{Ni}_{48.8}\text{Mn}_{34}\text{In}_{17.2}$ (within ± 0.5 at. %) for the samples used in neutron scattering and ultrasonic experiments, respectively.

B. Calorimetric measurements

Structural and magnetic transitions of the samples were characterized by means of differential scanning calorimetry (DSC) measurements. Calorimetric measurements were carried out in the temperature range 150

$\text{K} \leq T \leq 375$ K in a DSC (TA Instruments MDSC 2920) at cooling and heating rates of 5 K/min. We have also used a second high sensitivity calorimeter for measurements in the temperature range $100 \text{ K} \leq T \leq 350$ K. In this case, typical cooling and heating rates were 0.5 K/min.

C. Neutron scattering

The crystals used in the experiments were cut from a large boule to a size allowing mounting in the various sample environment systems. A side benefit of this was a larger surface-to-volume ratio, important because of the large absorption cross section of In for thermal neutrons (194 bn). The samples were still sizeable (~ 4 and ~ 6 cm^3) although not perfect single crystals. Rocking curves of the (220) Bragg reflections used for sample orientation showed, in one case, a secondary peak, which was very close to the primary peak ($< 1^\circ$ away) and, in the other case, a secondary peak with much lower intensity than the primary peak ($\sim 20\%$). Peak-widths of the (220) rocking curves were from 0.5° to 1° . The secondary peaks warranted caution in interpretation of the data but were not prohibitive in performing the experiments.

The inelastic neutron scattering experiments were performed using the HB1A triple-axis spectrometer at the High Flux Isotope Reactor (HFIR) of the Oak Ridge National Laboratory (ORNL). The monochromator and analyzer used the (002) reflection of pyrolytic graphite (PG). Highly oriented PG filters (HOPG) were used to minimize higher-order contaminations of the beam. The HB1A spectrometer operates at a fixed incident energy of 14.6 meV requiring most scans to be performed with neutron-energy gain. Nominal collimations of $48'-48'-40'-68'$ (or $136'$) were used and all scans were performed in the constant-Q mode while counting against neutron monitor counts.

The temperature dependent dispersion curve measurements were made in a closed-cycle helium refrigerator (CCHR) with a high temperature interface unit enabling the sample to be warmed to temperatures above room temperature. Temperature control was better than ± 1 K and accuracy, due to temperature sensor location, $\sim \pm 5$ K. The magnetic field measurements were made in a conventional superconducting cryomagnet with temperature control again to within ± 1 K. The sample location on the HB1A triple-axis spectrometer which is near the massive and magnetic monochromator drum of the HB1 triple-axis spectrometer, requires limiting applied magnetic fields to ~ 4 T.

D. Ultrasonic methods

The single crystal was oriented in the austenite phase by Laue back reflection, and a parallelepiped specimen with dimensions $5.0 \times 5.0 \times 3.7$ mm^3 with faces paral-

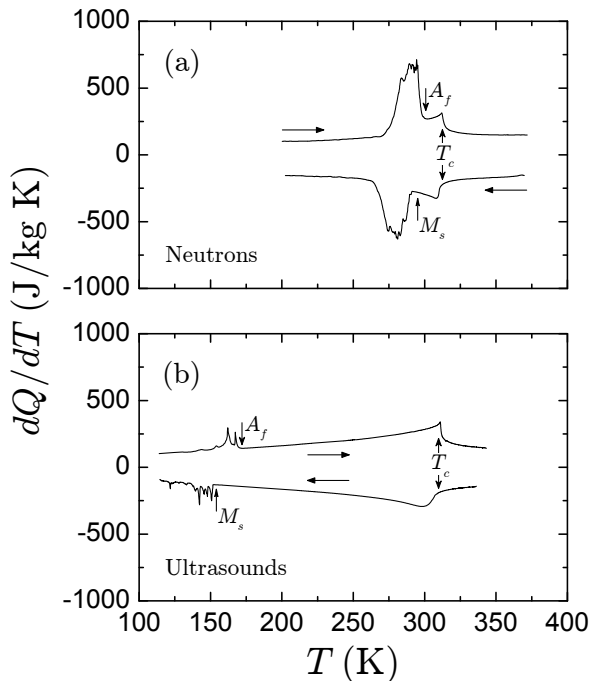


FIG. 1: Calorimetric curves for the samples used in (a) neutron scattering ($\text{Ni}_{49.3}\text{Mn}_{34.2}\text{In}_{16.5}$) and (b) ultrasonic measurements ($\text{Ni}_{48.8}\text{Mn}_{34}\text{In}_{17.2}$). Vertical arrows show the position of martensitic and Curie transition temperatures. Heating and cooling runs are shown with horizontal arrows.

lel to the $(1\bar{1}0)$, (110) , and (001) planes, respectively, was spark cut from the oriented boule. The faces were ground parallel and flat using standard metallographic techniques.

The velocity of ultrasonic waves was determined by the pulse-echo technique. X-cut and Y-cut transducers with resonant frequencies of 10 MHz were used to generate and detect the ultrasonic waves. The transducers were acoustically coupled to the surface of the sample by means of Dow Corning Resin 276-V9 in the temperature range 200–320 K and by Crystalbond509 (Aremco Products, Inc.) in the temperature range 310–360 K. For high-temperature measurements (up to 360 K), the sample was placed into a copper sample holder which was heated by means of a heating plate. For low-temperature measurements (down to 200 K), the sample and sample holder were introduced into a dewar glass containing liquid nitrogen. In both cases, the temperature was measured by a Ni-Cr/Ni-Al thermocouple attached to the sample.

The measurements of the magnetic field dependence of the elastic constants were carried out in a purpose-built device that allows both isofield and isothermal measurements of the ultrasonic velocities in applied fields up to 1.3 T (details are given in reference [19]). The measurements were carried out at constant temperature and the magnetic field was applied perpendicular to the propagation direction of the ultrasonic waves.

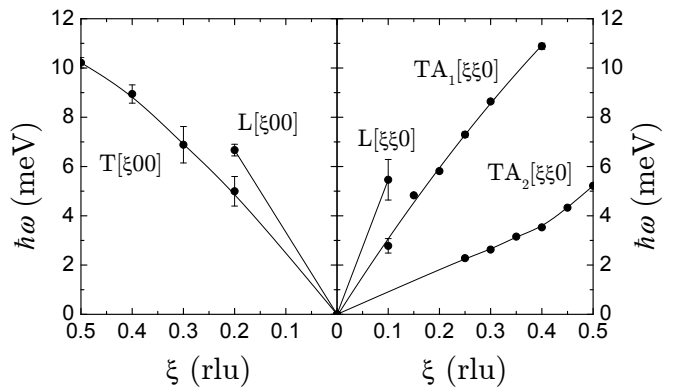


FIG. 2: Acoustic phonon dispersion curves along the high-symmetry directions $[\xi 00]$ and $[\xi \xi 0]$ measured at 520 K. Solid lines are guides to the eye.

III. EXPERIMENTAL RESULTS AND DISCUSSION

A. Calorimetry

We carried out calorimetric measurements in order to characterize the samples to be studied in the neutron scattering and ultrasonic experiments.

Calorimetric studies were carried out on small pieces of samples cut using a low speed diamond saw from the top and bottom of the large ingot (~ 7 cm long), which was used in the neutron scattering experiments. For the sample cut from the top of the ingot [Fig. 1(a)], calorimetric studies revealed both a ferromagnetic transition at the Curie temperature $T_C = 312$ K and a martensitic transformation at a lower temperature with characteristic temperature $(M_s + A_f)/2 \approx 297$ K (M_s : martensite-start; A_f : austenite-finish). Measurements for the sample cut from the bottom yielded similar results with a shift of the transition temperatures of approximately 10 K to higher values – the shift of the structural transitions being slightly larger than the shift of the Curie point. These discrepancies are ascribed to small changes on composition through the length of the ingot.

Similar measurements carried out in the parallelepiped specimen used in the ultrasonic experiments revealed a ferromagnetic transition at $T_C = 310$ K and a martensitic transformation at lower temperatures with characteristic temperature $(M_s + A_f)/2 \approx 161$ K [Fig. 1(b)].

B. Phonon dispersion

Figure 2 shows the phonon dispersion curves determined from inelastic neutron scattering at 520 K along the high-symmetry directions $[\xi 00]$ and $[\xi \xi 0]$. Note that the plot of dispersion curves is restricted to half of the Brillouin zone scheme. The measured phonon spectrum shows the features typical of bcc materials that undergo martensitic transformations, i.e., low energies of the

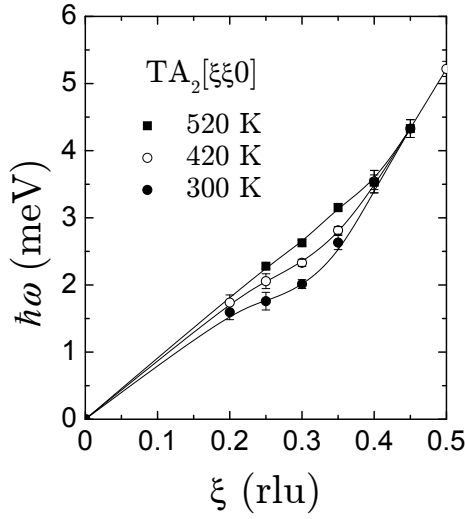


FIG. 3: Temperature dependence of the $TA_2[\xi\xi 0]$ branch. The wiggle at $\xi_0 \approx 0.33$ deepens with decreasing temperature thus reflecting the softening of the anomalous phonon. Solid lines are guides to the eye.

phonons of the transverse $TA_2[\xi\xi 0]$ branch and a wiggle at $\xi_0 \approx 0.33$. A similar behavior has also been reported for the related systems Ni-Mn-Ga and Ni-Mn-Al with compositions close to stoichiometry [10, 11, 12, 13, 14]. The existence of such an anomaly in the transverse TA_2 branch is ascribed to a strong electron-phonon coupling and the Kohn anomaly [25].

In order to study the temperature dependence of the anomaly observed in the transverse TA_2 branch, we measured this dispersion curve at several temperatures down to room temperature, i.e., just above the structural transition. The results are shown in Figure 3. For sake of clarity, measurements only at three temperatures are presented. As can be seen from the figure, as the temperature is reduced, the energy of the branch close to the anomalous phonon decreases, thus reflecting the dynamical instability of the cubic lattice against distortions of $\{110\}$ planes along $\langle 1\bar{1}0 \rangle$ directions. It should be noted that despite of the fact that the sample transforms martensitically near room temperature, the wiggle present at high temperatures does not develop into a marked dip even at 300 K. This behaviour differs from that observed in Ni-Mn-Ga alloys [10, 11, 12, 13] but is similar to that previously reported in a Ni-Mn-Al alloy close to stoichiometry [14].

In order to compare the behaviour of the different Ni-Mn based systems, we have plotted in Fig. 4 the energy squared of the anomalous phonons as a function of temperature for different compounds. Additionally, data for the soft phonon in $Ni_{62.5}Al_{37.5}$ alloy are also plotted. As can be seen from the figure, the degree of softening in the studied sample is similar to that of $Ni_{62.5}Al_{37.5}$ and $Ni_{54}Mn_{23}Al_{23}$, although the energy values of the latter are higher, which is consistent with the fact that the Ni-Mn-Al sample does not transform martensitically within

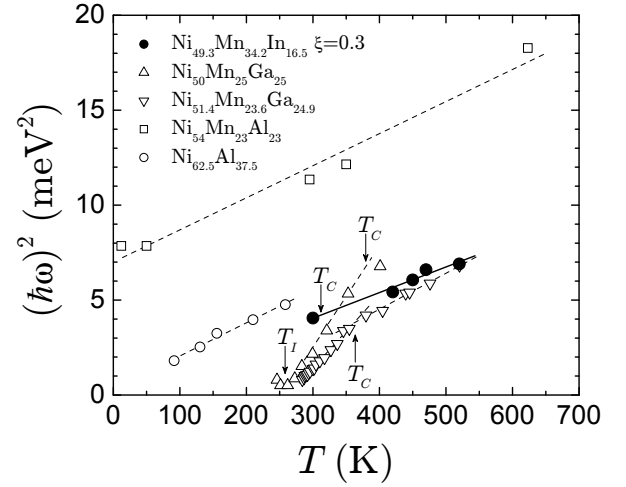


FIG. 4: Temperature dependence of the energy squared of the $TA_2[\xi\xi 0]$ phonon modes close to the anomalous phonon, $\xi = 0.3$ (filled circles). Data from related systems Ni_2MnGa , $Ni_{54}Mn_{23}Al_{23}$ and $Ni_{62.5}Al_{37.5}$ are also shown for comparison. T_l represents the premartensitic transition temperature. The data for the latter systems were taken from references [11], [12], [14] and [26] for $Ni_{50}Mn_{25}Ga_{25}$, $Ni_{51.4}Mn_{23.6}Ga_{24.9}$, $Ni_{54}Mn_{23}Al_{23}$ and $Ni_{62.5}Al_{37.5}$, respectively. Lines are linear fits to the experimental data.

the studied temperature range. By contrast, Ni_2MnGa alloys show a more complex behaviour. While the degree of softening in the paramagnetic state is similar to the studied sample and to the other related alloys, the softening below the Curie point is much stronger. This is due to strong spin-phonon coupling exhibited by these compounds in the ferromagnetic state [27, 28]. It should be noted that despite the studied Ni-Mn-In sample is also ferromagnetic, changes in the degree of softening below T_C were not discernible due to the closeness of the magnetic and the structural transitions.

The measured dispersion curves are in good agreement with those obtained from *ab initio* calculations for the $[110]$ direction in Ni_2MnIn [22], except for the low energy transverse TA_2 branch, which exhibits complete softening in the range between $\xi = 0.25$ and $\xi = 0.45$. Experimental data are in agreement with such an instability and show that the minimum is located at $\xi_0 \approx 0.33$. However, it can be seen from Fig. 3 that the softening is not complete, i.e., the phonon frequency remains finite even at the lowest temperatures.

As mentioned above, the large shift of the structural martensitic transition with the applied magnetic field in these compounds enables the phase transition to be induced by applying a magnetic field [5]. The microscopic origin of such strong dependence of the transition temperature on the magnetic field is ascribed to a strong magnetoelastic coupling, which is responsible for the change in the relative stability of the martensitic and cubic phases when the field is applied. Actually, recent *ab initio* calculations at 0 K for cubic Ni_2MnIn have

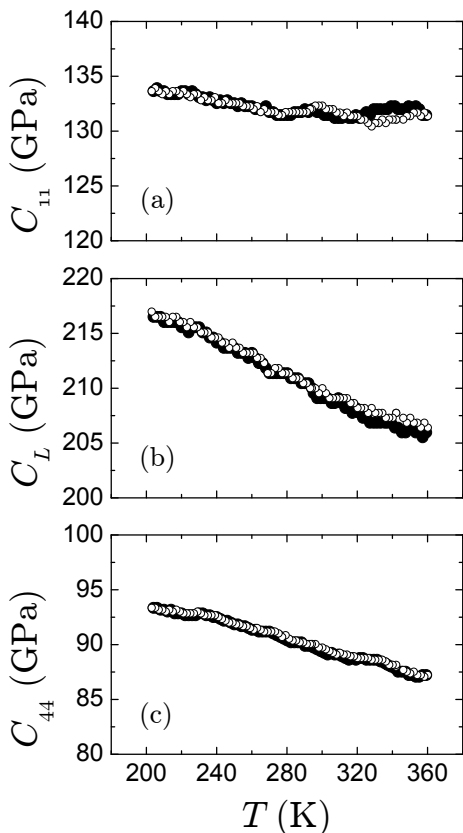


FIG. 5: Temperature dependence of the elastic moduli (a) C_{11} , (b) $C_L = (C_{11} + C_{12} + 2C_{44})/2$, and (c) C_{44} . Open and solid symbols stands for cooling and heating runs, respectively.

shown that increasing the magnetization due to an external magnetic field leads to a gradual vanishing of the phonon instability due to the coupling between vibrational and magnetic degrees of freedom [23]. We measured the transverse phonon branch TA_2 in the region close to the anomalous phonon at several applied magnetic fields and at temperatures slightly above the structural transition. Our results show no significant changes of the phonon energy with the applied field, so that for these applied fields, the results cannot confirm the *ab initio* predictions. However, it should be noted that the magnetic fields involved in the calculations are considerably larger than the fields attainable experimentally in our measurements [29]. Moreover, it should be also noted that the close proximity of the magnetic and structural transitions in $Ni_{49.3}Mn_{34.2}In_{16.5}$ could inhibit the development of the necessary strong magnetoelastic coupling before the martensitic transformation takes place and, hence, prevent the observation of the predicted magnetic field induced behaviour.

C. Elastic constants

In order to complement the study in the long-wavelength range, we have measured the elastic constants using the pulse-echo technique. The results of the temperature-dependent elastic constants measurements are shown in Fig. 5, where the thermal behaviour of the three independent elastic constants C_{11} , C_L , and C_{44} is shown. These are computed from ultrasonic waves propagating along the [001] and [110] directions down to temperatures close to the martensitic transformation. The data correspond to cooling (open circles) and heating (solid circles) runs and are obtained as an average over several independent runs. As can be seen from the figure, all three elastic constants increase with decreasing temperature reflecting the stiffening of the lattice as the temperature is lowered. C_{11} depends weakly on temperature, similar to the behaviour reported for the related systems Ni-Mn-Ga [18] and Ni-Mn-Al [19]. Additionally, it should be noted that the elastic moduli show no significant changes at the Curie point, $T_C = 310$ K. This behaviour agrees with that reported in the ferromagnetic Ni-Mn-Ga alloys [18] but differs from the behaviour displayed by the antiferromagnetic Ni-Mn-Al system. In the latter case, antiferromagnetic ordering leads to a decrease of the elastic constants [19]. We also note that similar features have been observed in other antiferromagnetic systems such as chromium [30], Fe-Mn and Co-Mn [31, 32] below their Néel temperatures. Thus, the type of magnetic order developed in the system appears to influence the elastic properties, although more studies are required in order to clarify this point.

From the complete set of measured elastic constants shown in Fig. 5 we can compute the temperature dependence of other relevant elastic moduli. Fig. 6(a) shows the temperature dependence of the shear elastic constant C' computed as $C_{11} + C_{44} - C_L$. Owing to the strong attenuation of the shear waves associated with this mode, it was not possible to obtain reliable echoes and therefore to measure C' directly. As can be seen from the figure, C' exhibits a low value and softens with decreasing temperature. Again, these features reflect the dynamical instability of the cubic lattice against shearing of {110} planes along $\langle 1\bar{1}0 \rangle$ directions. Additionally, Fig. 6(b) shows the temperature dependence of the elastic anisotropy calculated as $A = C_{44}/C'$. The elastic anisotropy at room temperature is similar to those reported for the related systems Ni-Mn-Ga [18] and Ni-Mn-Al [19], but significantly lower than for Cu-based shape memory alloys [33].

Up to now, we have discussed the behaviour of the elastic constants of the Ni-Mn-In alloy obtained from ultrasonic methods. Elastic constants can be also derived from the initial slope ($\xi \rightarrow 0$) of the acoustic phonon branches reported in section III B. Table I summarizes the elastic constants obtained from both experiments. As can be seen, both methods agree well on the values of C_{44} and C' . There is less agreement on the values for the longitudinal constants C_{11} and C_L , which correspond to

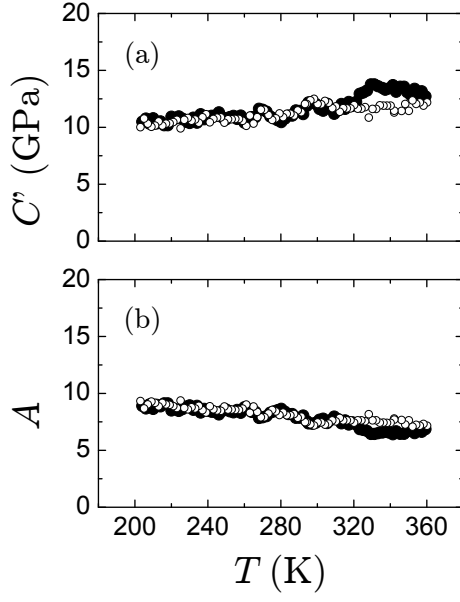


FIG. 6: (a) Temperature dependence of the shear elastic constant C' ($= C_{11} + C_{44} - C_L$) and (b) the elastic anisotropy $A = C_{44}/C'$ calculated from the complete set of measured elastic constants (shown in figure 5). Open and solid symbols stands for cooling and heating runs, respectively.

TABLE I: Elastic constants obtained both from ultrasonic methods at 300 K and from the initial slopes of the acoustic phonon branches ($\xi \rightarrow 0$) at 520 K. Values determined experimentally show the associated uncertainty. The calculated values, corresponding to the stoichiometric Ni_2MnIn sample, were estimated from the phonon branches obtained from *ab-initio* calculations (reference [22]).

	Ultrasonics (GPa)	Neutrons (GPa)	<i>Ab-initio</i> (GPa)
C_{11}	132 ± 8	190 ± 15	121
C_L	210 ± 10	260 ± 50	207
C_{44}	90 ± 3	90 ± 15	101
C'	12	12 ± 4	15

the initial slope of the $L[\xi 00]$ and $L[\xi \xi 0]$ branches, respectively, for which the values obtained from the dispersion branches are affected by a large error due to limited experimental data. Additionally, our experimental results are in good agreement with elastic constants obtained from first-principles calculations in the stoichiometric Ni_2MnIn [22]. Again, discrepancies may arise from the definition of the initial slope, but note that these can also arise from changes in sample composition and temperature.

Finally, to investigate further the interplay between elastic and magnetic properties, we measured the elastic constants as a function of applied magnetic field at constant temperature. Results presented in Fig. 7 show the magnetic-field dependence of the relative change of

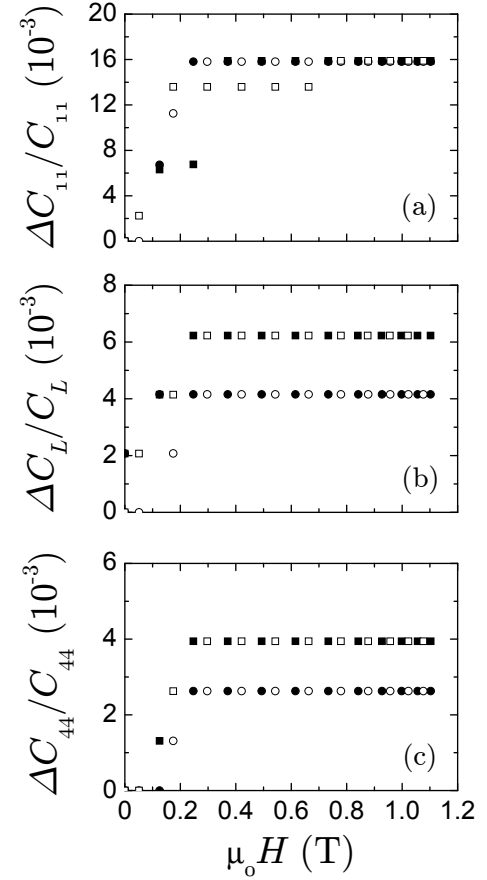


FIG. 7: Magnetic-field dependence of the relative change of the elastic constants with respect to the value at zero field at $T = 260$ K. (a) C_{11} versus applied magnetic field along $[110]$ (circle symbols) and $[1\bar{1}0]$ (square symbols). (b) C_L versus applied magnetic field along $[001]$ (circle symbols) and $[110]$ (square symbols). (c) C_{44} versus applied magnetic field along $[001]$ (circle symbols) and $[1\bar{1}0]$ (square symbols). Solid and open symbols correspond to increasing and decreasing magnetic field runs, respectively.

the elastic constants at $T = 260$ K with respect to the zero-field value. The temperature is located well below the Curie point of the studied sample, $T_C = 310$ K. Note that in this case, the ferromagnetic and the structural transitions are well separated [Fig. 1(b)] and thus significant magnetoelastic coupling is expected in contrast to the case for the sample studied by means of neutron scattering experiments (Sec. IIIB). As can be seen from the figure, all elastic constants increase up to a saturation value with increasing magnetic field. This behaviour is similar to that reported for the prototypical ferromagnetic shape memory alloy Ni-Mn-Ga [21] but differs from the observed behaviour in the antiferromagnetic Ni-Mn-Al system, which shows an anisotropic magnetoelastic coupling [19]. As discussed before, the type of magnetic order present in the different compounds of the Ni-Mn based family influences their elastic properties, as reflected by the different temperature dependence of the

elastic constants across the magnetic transition [18, 19]. Additionally, the magnetic field dependence of the elastic moduli further evidences the dependence of the elastic properties on the type of magnetic ordering indicating that the magnetic order also determines the magnetoelastic response of these alloy systems [19, 21].

IV. SUMMARY AND CONCLUSIONS

We have carried out neutron scattering and ultrasonic experiments in order to study in detail the lattice dynamics of Ni-Mn-In Heusler alloys with composition close to the $\text{Ni}_{50}\text{Mn}_{34}\text{In}_{16}$ magnetic superelastic alloy. In order to study the interplay between dynamical and magnetic degrees of freedom, we performed both kind of experiments in applied magnetic fields. The most relevant outcomes from this study are:

- The values obtained for the elastic constants from both neutron scattering and ultrasonic experiments are in good agreement with each other. In addition, data reported for the stoichiometric Ni_2MnIn from *ab initio* calculations are consistent with the measured values.
- The TA_2 phonon branch exhibits a wiggle in the vicinity of $\xi_0 \approx 1/3$ at temperatures well above the Curie point. Upon cooling this anomaly is enhanced, but even at temperatures close to the martensitic transition the dip is less pronounced than in Ni-Mn-Ga.
- The elastic constant C' also softens with decreasing temperature down to the martensitic transition. Both

the anomalous phonon energy and C' have finite values at the transition temperature. The monotonic decrease in the anomalous phonon energy and in the elastic constant indicate the absence of a premartensitic phase (associated with the condensation of the anomalous phonon) in this alloy system.

- Within experimental errors, the development of ferromagnetic order at the Curie point does not modify the rate of softening.

- While no magnetic field dependence of phonon energies has been measured for fields up to 4 T, all elastic constants increase with increasing magnetic field thus evidence the existence of magnetoelastic coupling at the long-wavelength limit.

Acknowledgments

This work received financial support from the CICyT (Spain), Project No. MAT2007-62100 and from the Deutsche Forschungsgemeinschaft (SPP 1239). XM acknowledges support from Comissionat per a Universitats i Recerca (CUR) del Departament d'Innovació, Universitat i Empresa de la Generalitat de Catalunya. Experiments at Oak Ridge National Laboratory's High Flux Isotope Reactor was sponsored by the Scientific User Facilities Division, Office of Basic Energy Sciences, U. S. Department of Energy. Work at the Ames Laboratory was supported by the Office of Basic Energy Sciences USDOE, under Contract No. DE-AC02-07CH11358.

-
- [†] Present address: Department of Materials Science and Metallurgy, University of Cambridge, Pembroke Street, Cambridge CB2 3QZ, UK.
- [1] Y. Sutou, Y. Imano, N. Koeda, T. Omori, R. Kainuma, K. Ishida, and K. Oikawa, Appl. Phys. Lett. **85**, 4358 (2004).
 - [2] T. Krenke, M. Acet, E. F. Wassermann, X. Moya, L. Mañosa, and A. Planes, Phys. Rev. B **72**, 014412 (2005).
 - [3] T. Krenke, M. Acet, E. F. Wassermann, X. Moya, L. Mañosa, and A. Planes, Phys. Rev. B **73**, 174413 (2006).
 - [4] T. Krenke, M. Acet, E. F. Wassermann, X. Moya, L. Mañosa, and A. Planes, Nat. Mater. **4**, 450 (2005).
 - [5] T. Krenke, E. Duman, M. Acet, E. F. Wassermann, X. Moya, L. Mañosa, A. Planes, E. Suard, and B. Ouladdiaf, Phys. Rev. B **75**, 104414 (2007).
 - [6] Z. D. Han, D. H. Wang, C. L. Zhang, S. L. Tang, B. X. Gu, and Y. W. Du, Appl. Phys. Lett. **89**, 182507 (2006).
 - [7] X. Moya, L. Mañosa, A. Planes, S. Aksoy, T. Krenke, M. Acet, and E. F. Wassermann, Phys. Rev. B **75**, 184412 (2007).
 - [8] A. Planes, L. Mañosa and M. Acet, J. Phys.: Condens. Matter **21**, 233201 (2009).
 - [9] V. K. Sharma, M. K. Chattopadhyay, K. H. B. Shaeb, A. Chouhan, and S. B. Roy, Appl. Phys. Lett. **89**, 222509 (2006).
 - [10] A. Zheludev, S. M. Shapiro, P. Wochner, A. Schwartz, M. Wall, and L. E. Tanner, Phys. Rev. B **51**, 11310 (1995).
 - [11] A. Zheludev, S. M. Shapiro, P. Wochner, and L. E. Tanner, Phys. Rev. B **54**, 15045 (1996).
 - [12] U. Stühr, P. Vorderwisch, V. V. Kokorin, and P.-A. Lindgård, Phys. Rev. B **56**, 14360 (1997).
 - [13] L. Mañosa, A. Planes, J. Zarestky, T. Lograsso, D. L. Schlagel, and C. Stassis, Phys. Rev. B **64**, 024305 (2001).
 - [14] X. Moya, L. Mañosa, A. Planes, T. Krenke, M. Acet, V. O. Garlea, T. A. Lograsso, D. L. Schlagel, and J. L. Zarestky, Phys. Rev. B **73**, 064303 (2006).
 - [15] T. Mehaddene, J. Neuhaus, W. Petry, K. Hradil, P. Bourges, and A. Hiess, Phys. Rev. B **78**, 104110 (2008).
 - [16] J. Worgull, E. Petti, and J. Trivisonno, Phys. Rev. B **54**, 15695 (1996).
 - [17] L. Mañosa, A. González-Comas, E. Obradó, A. Planes, V. A. Chernenko, V. V. Kokorin, and E. Cesari, Phys. Rev. B **55**, 11068 (1997).
 - [18] M. Stipcich, L. Mañosa, A. Planes, M. Morin, J. Zarestky, T. Lograsso, and C. Stassis, Phys. Rev. B **70**, 054115 (2004).
 - [19] X. Moya, L. Mañosa, A. Planes, T. Krenke, M. Acet, M. Morin, O. V. Garlea, T. A. Lograsso, and J. Zarestky, Phys. Rev. B **74**, 024109 (2006).
 - [20] A. Planes and L. Mañosa, Solid State Phys. **55**, 159 (2001).
 - [21] A. González-Comas, E. Obradó, L. Mañosa, A. Planes, V. A. Chernenko, B. J. Hattink, and A. Labarta, Phys. Rev. B **60**, 7085 (1999).

- [22] A. T. Zayak, P. Entel, K. M. Rabe, W. A. Adeagbo, and M. Acet, Phys. Rev. B **72**, 054113 (2005).
- [23] P. Entel, M. E. Gruner, W. A. Adeagbo, and A. T. Zayak, Mater. Sci. Engn. A **481-482**, 258 (2008).
Okamoto, O. Kitakami, K. Oikawa, A. Fujita, T. Kanomata and K. Ishida,
Rev. B **76**, 140401(R) (2007).
- [24] Materials Preparation Center, Ames Laboratory, Ames, IA 50011 (see www.mpc.ameslab.gov).
- [25] Y. Lee, J. Y. Rhee, and B. N. Harmon, Phys. Rev. B **66**, 054424 (2002).
- [26] S. M. Shapiro, B. X. Yang, Y. Noda, L. E. Tanner, and D. Schryvers, Phys. Rev. B **44**, 9301 (1991).
- [27] A. Planes, E. Obradó, A. González-Comas, and L. Mañosa, Phys. Rev. Lett. **79**, 3926 (1997).
- [28] M. A. Uijttewaalt, T. Hickel, J. Neugebauer, M. E. Gruner, and P. Entel, Phys. Rev. Lett. **102**, 035702 (2009).
- [29] M. E. Gruner, private communication.
- [30] W. C. Muir, J. M. Perz, and E. Fawcett, J. Phys. F: Met. Phys. **17**, 2431 (1987).
- [31] M. Cankurtaran, G. A. Saunders, P. Ray, Q. Wang, U. Kawald, J. Pelzl, and H. Bach, Phys. Rev. B **47**, 3161 (1993).
- [32] U. Kawald, O. Mitze, H. Bach, J. Pelzl, and G. A. Saunders, J. Phys.: Condens. Matter **6**, 9697 (1994).
- [33] A. Planes, L. Mañosa, and E. Vives, Phys. Rev. B **53**, 3039 (1996).